Molecular Biology of the Cell
Vol. 21, 2721–2731, August 1, 2010

Identification of Three Distinct Functional Sites of Insulin-mediated GLUT4 Trafficking in Adipocytes Using Quantitative Single Molecule Imaging

Hideaki Fujita,*† Hiroyasu Hatakeyama,†‡ Tomonobu M. Watanabe,*§ Masaaki Sato,‡ Hideo Higuchi,*‖ and Makoto Kanzaki*‡¶

*Tohoku University Biomedical Engineering Research Organization, Sendai, Miyagi, 980-8575, Japan; ‡Graduate School of Biomedical Engineering, Tohoku University, Sendai, Miyagi, 980-8575, Japan; §World Premier International Research Center, Immunology Frontier Research Center, Osaka University, Suita, Osaka, 565-0871, Japan; ‖Department of Physics, Graduate School of Science, University of Tokyo, Tokyo, 113-0033, Japan; and ¶Core Research for Evolutional Science and Technology (CREST), Japan Science and Technology Agency, Kawaguchi, Saitama, 332-0012, Japan

Submitted January 12, 2010; Revised April 30, 2010; Accepted May 20, 2010
Monitoring Editor: Thomas F.J. Martin

Insulin stimulation of glucose uptake is achieved by redistribution of insulin-responsive glucose transporters, GLUT4, from intracellular storage compartment(s) to the plasma membrane in adipocytes and muscle cells. Although GLUT4 translocation has been investigated using various approaches, GLUT4 trafficking properties within the cell are largely unknown. Our novel method allows direct analysis of intracellular GLUT4 dynamics at the single molecule level by using Quantum dot technology, quantitatively establishing the behavioral nature of GLUT4. Our data demonstrate the predominant mechanism for intracellular GLUT4 sequestration in the basal state to be "static retention" in fully differentiated 3T3L1 adipocytes. We also directly defined three distinct insulin-stimulated GLUT4 trafficking processes: 1) release from the putative GLUT4 anchoring system in storage compartment(s), 2) the speed at which transport GLUT4-containing vesicles move, and 3) the tethering/docking steps at the plasma membrane. Intriguingly, insulin-induced GLUT4 liberation from its static state appeared to be abolished by either pretreatment with an inhibitor of phosphatidylinositol 3-kinase or overexpression of a dominant-interfering AS160 mutant (AS160/T642A). In addition, our novel approach revealed the possibility that, in certain insulin-resistant states, derangements in GLUT4 behavior can impair insulin-responsive GLUT4 translocation.

INTRODUCTION

Under normal physiological conditions, insulin prevents postprandial increases in blood glucose levels by increasing glucose uptake into adipose and muscle cells. The insulin-responsive glucose transporter 4 (GLUT4) is predominantly expressed in tissues that display the highest levels of insulin-dependent glucose uptake (James *et al*., 1988; Birnbaum, 1989). Under basal conditions, ~95% of GLUT4 protein is localized within intracellular membrane compartments, with the remaining 5% at the cell surface (Martin *et al*., 2000). This is in marked contrast to proteins in the general recycling pathway, such as the transferrin receptor (TfR) (Livingstone *et al*., 1996). These observations together with other experimental evidence establish a selective retention mechanism that efficiently sequesters GLUT4 within specialized postendosomal membrane compartments, including a subdomain of the *trans*-Golgi network (TGN; Shewan *et al*., 2003). By contrast, insulin triggers a major GLUT4 redistribution from intracellular storage sites to the plasma membrane, accounting for large insulin-stimulated increases in glucose uptake (Cushman and Wardzala, 1980; Suzuki and Kono, 1980). Importantly, impaired GLUT4 translocation to the plasma membrane has been implicated as one of the earliest defects leading to the development of insulin resistance and type 2 diabetes (Shepherd and Khan, 1999).

Despite this general understanding of insulin-stimulated glucose uptake, many unanswered questions remain, especially regarding the intracellular GLUT4 trafficking property, i.e., its behaviors under basal conditions as well as the actual steps at which insulin receptor signals directly converge and exert their effects. For example, GLUT4 can be retained via accumulation in a specific compartment in which it is immobile in the basal state but released upon insulin stimulation (static retention model) (Govers *et al*., 2004). Alternatively, GLUT4 could be sequestered via continuous release and recycling back into the insulin-responsive compartment in the basal state and insulin stimulation would then block the recycling step, thereby allowing GLUT4 to traffic to the plasma membrane (dynamic retention model) (Karylowski *et al*., 2004). Several studies have addressed this issue by extrapolating the recycling dynamics of total GLUT4 molecules obtained by measuring equilibrium distributions of the exofacial myc/HA-GLUT4 accessible to the cell surface during a certain period (Govers *et al*., 2004; Muretta *et al*., 2008). However, these indirect insights

This article was published online ahead of print in *MBoC in Press* (http://www.molbiolcell.org/cgi/doi/10.1091/mbc.E10–01–0029) on June 2, 2010.

† These authors contributed equally to this work.

Address correspondence to: Makoto Kanzaki (kanzaki@bme.tohoku.ac.jp).

© 2010 by The American Society for Cell Biology

provide a confusing picture and cannot delineate between the static retention and dynamic retention models (Govers *et al*., 2004; Karylowski *et al*., 2004), even under basal conditions. Much greater difficulties exist in specifying functional sites of insulin-mediated GLUT4 trafficking within cells, due to heterogeneous GLUT4 distributions and the complexity of their trafficking processes. Thus, it is impossible to separate intracellular GLUT4 trafficking processes into discrete experimentally traceable steps with ensemble imaging techniques.

In recent years, optical imaging techniques using a fluorescent semiconductor nanoparticle (Quantum dot; QD) have demonstrated that dynamic behaviors of single molecules can be analyzed in living cells, which was not possible using conventional biochemical and cell biological techniques (Dahan *et al*., 2003; Watanabe and Higuchi, 2007). To determine which GLUT4 trafficking step(s) is directly altered by insulin stimulation, we have used QD technology to quantitatively analyze GLUT4 movements in living 3T3L1 adipocytes. In addition, we also investigated GLUT4 trafficking properties in an insulin-resistant state.

MATERIALS AND METHODS

Materials

DMEM was purchased from Sigma-Aldrich (St. Louis, MO), and calf serum (CS) and fetal bovine serum (FBS) were purchased from BioWest (Miami, FL). Anti-myc antibody was purchased from Santa Cruz Biotechnology (Santa Cruz, CA), and the Fab fragment of the antibody was generated and purified with immobilized papain (Sigma-Aldrich) and an immobilized protein A column (Pierce Chemical, Rockford, IL), respectively. The QD antibody conjugation kit was purchased from Invitrogen (Carlsbad, CA), and the QD was conjugated with the Fab fragment of anti-myc antibody according to the manufacturer's instructions. The final concentration of the QD-conjugated antibody was determined by optical density at the specified wavelength according to the manufacturer's instructions. Conjugation of transferrin with QD was performed with transferrin-biotin and streptavidin-QD (Invitrogen) in the presence of excess (100×) amount of biotin to achieve single transferrin per QD (Serge *et al*., 2008). We used QD605 and QD655 for these experiments and found no significant differences in behavioral characteristics. Anti-phosphorylated Akt (Ser^{473}) and anti-Akt antibodies, anti-insulin-responsive aminopeptidase (IRAP) antibodies and Alexa555-conjugated anti-rabbit immunoglobulin (Ig)G were from Cell Signaling Technology (Danvers, MA), Alpha Diagnostic International (San Antonio, TX), and Invitrogen, respectively. Human TfR cDNA was subcloned into pcDNA3. Expression vector containing cDNA encoding AS160 (Tbc1d4) fused to HaloTag (pFN21AA0603) was purchased from Promega K.K. Japan (Tokyo, Japan), and a point mutation (T642A) was introduced by the polymerase chain reaction (PCR)-based method using 5′-GAAGACGGGCACACGCGTTCAGCCACCCACC-3′ and 5′-GGTGGGTGGCTGAAACGCGTGTGCCCGTCTTC-3′. The mutated nucleotide sequence was confirmed by ABI PRISM 3130 Genetic Analyzer (Applied Biosystems, Foster City, CA). The Western blot detection kit (West Super Femto Detection reagents) was from Pierce Chemical. All other chemicals were of reagent grade.

Cell Culture

3T3L1 fibroblasts were transfected with an expression vector containing cDNA encoding myc-GLUT4-ECFP, possessing the myc tag at the first exofacial loop and enhanced cyan fluorescent protein (ECFP) at the C terminus of GLUT4 (Nedachi and Kanzaki, 2006). Cells expressing low-moderate levels of myc-GLUT4-ECFP were selected, cloned and cultured in DMEM containing 4.5 g l^{-1} glucose and 10% CS at 37°C in an 8% CO_2 atmosphere. For the experiments, cells were cultured on a glass-bottomed recording chamber (thickness, 0.15–0.18 mm; Matsunami-glass, Osaka, Japan) and differentiated after reaching confluence in DMEM containing 10% FBS, 500 μM isobutylmethylxanthine, 25 μM dexamethasone, and 4 μg ml^{-1} insulin. After 4 d, the medium was removed and replaced with DMEM containing 10% FBS, 4.5 g l^{-1} glucose, and 4 μg ml^{-1} insulin. After a further 2–4 d in culture, the cells were used for the experiments. In some experiments, differentiated cells (day 6) were replated in glass-bottomed recording chambers and further cultured for one additional day for observation. We found no significant differences in GLUT4 movement between culture conditions. Three different stable clones expressing myc-GLUT4-ECFP were studied. In some experiments, transient transfection was also carried out by previously described electroporation methods (Kanzaki and Pessin, 2001). For endothelin (ET)-1 experiments, differentiated cells were treated with 10 ng/ml^{-1} ET-1 for 16 h and then subjected to the single particle tracking study.

Single Particle Tracking of GLUT4

For labeling of GLUT4, the differentiated adipocytes expressing myc-GLUT4-ECFP were serum starved and stimulated with 1–10 nM insulin in the presence of QD-conjugated Fab fragment of anti-myc antibody for 60 min. In most cases, concentration of the QD-conjugated antibodies was 1.5 nM, but we used 10-fold higher concentrations of the antibodies in some experiments. The cells were then extensively washed to remove excess insulin and unbound QD-labeled antibodies, followed by an additional incubation for 4 h to allow the QD-labeled myc-GLUT4-ECFP molecules to undergo endocytosis and recycle back into the GLUT4 storage compartments (see Figure 1A). Consistent with previous reports using anti-myc or hemagglutinin (HA) antibody to label the myc-/HA-tagged GLUT4 (Shigematsu *et al*., 2002; Karylowski *et al*., 2004), labeling with QD-labeled antibodies did not interfere with myc-GLUT4-ECFP translocation in response to a second insulin stimulation (Supplemental Figure S1 and S2B). QD spots consistently colocalized and moved together with ECFP fluorescence emitted by the myc-GLUT4-ECFP (Supplemental Figure S1, C and D). However, QD fluorescence was highly resistant to photobleaching as compared with ECFP (Supplemental Figure S1E). The distribution of fluorescence intensities of QD spots was well fitted with the sum of multiple Gaussian functions, and the mean of the first component and interpeak spacing of the Gaussian functions were almost identical to the blinking amplitude (Supplemental Figure S1, F and G), suggesting that the fluorescent signals reflect one, two, or more QD. Because more than half the fluorescent signals belonged to the first component, we considered it most likely that this component contained a single QD. For labeling of TfR (Shigematsu *et al*., 2003), adipocytes overexpressing TfR were treated with transferrin-QD conjugates for 15 min, and images were acquired for up to 30 min.

Fluorescent Imaging

Imaging experiments were performed with an inverted microscope (model IX71; Olympus, Tokyo, Japan) equipped with a Nipkow disk confocal unit (CSU-10; Yokogawa, Tokyo, Japan) and an oil immersion objective lenses (APON 60×OTIRF, numerical aperture [NA] 1.49 [Olympus] or UPLSAPO100× O, NA 1.40 [Olympus]) at ~30°C in phenol red-free DMEM. Excitation and filters were as follows: ECFP, 405 nm excitation, emission band-pass (BP) 490 ± 10 nm filter; QD605, 532 nm excitation, emission BP 610 ± 10 nm filter; and QD655, 532 nm excitation, emission BP 655 ± 12 nm filter. Images were acquired with an electron multiplying charge-coupled device camera (iXon 887; Andor Technology, South Windsor, CT; 512 × 512 pixels) at 30 frames s^{-1}. Images were always acquired at ~2–4 μm above the glass surface. In experiments shown in Supplemental Figures S1 and S2, imaging was performed with an inverted microscope (model IX81; Olympus) equipped with a laser scanner (FV1000; Olympus) and an oil immersion objective lens (PlanApo 60×, NA 1.40). ECFP and Alexa555 were excited at 458 and 543 nm, respectively. QD were excited at 458 or 543 nm. The fluorescence of ECFP, Alexa555, QD605, and QD655 was measured at 480–495, 560–620, 560–620, and >610 nm, respectively. Indirect immunofluorescence staining was performed as described previously (Ariga *et al*., 2008).

Data Analysis

To track and analyze QD fluorescence trajectories, we used G-Track and G-Count software (G-Angstrom, Sendai, Japan) with which the *x-y* position of QD was calculated by fitting the fluorescent images with a two-dimensional Gaussian function (Tada *et al*., 2007; Watanabe and Higuchi, 2007). We analyzed the fluorescent spot that could be fitted with the two-dimensional Gaussian function within an 8 × 8 pixel region of interest (ROI) in which tracking for >30 frames (>1 s) was feasible. Thus, any fluorescent spot exceeding the ROI size ($\varphi > 1$ μm) or that differed significantly from the usual round shape, e.g., had a rod-like shape, was omitted from the analysis. Our system is capable of detecting the fluorescence of a single QD, and based on this single QD fluorescent intensity, we observed that a GLUT4 vesicle usually contains one to three QDs (Supplemental Figure S1G). The speeds of moving myc-GLUT4-ECFP molecules were calculated by linear fit of GLUT4 vesicle movement during four frames. If movement within the period was completely random, the velocity distribution $f(\boldsymbol{V})$ should follow the Gaussian function

$$f(\boldsymbol{V}) = \boldsymbol{A_0} \exp\left(-\frac{V^2}{2\sigma^2}\right) \tag{1}$$

where $\boldsymbol{A}_0$ and σ are numbers of particles with a velocity of zero and the SD, respectively. In two-dimensional movement, numbers of particles with speeds between V_S and $V_S + dV$, N, are proportional to

$$N \propto \pi(V_S + dV)^2 - \pi V_S^2 \approx 2\pi V_S dV \tag{2}$$

Thus, when dV is constant, the numbers of particles with the same speed V_S, $F(V_S)$, are described as

$$F(V_S) = N \cdot f(V_S) = AV_S \exp\left(-\frac{V_S^2}{2\sigma^2}\right) \tag{3}$$

where A is constant. In fact, we found that the speed distributions were best fitted with the function which has two components:

$$F(V_S) = A_1 V_S \exp\left(-\frac{V_S^2}{2\sigma_1^2}\right) + A_2 V_S \exp\left(-\frac{V_S^2}{2\sigma_2^2}\right) \quad (4)$$

where σ_1 and σ_2 are the apparent standard deviations of the immobile and mobile components, respectively. The SD of our experimental set-up was 6 nm per 33 ms = 0.182 μm s^{-1} (Watanabe and Higuchi, 2007). As noted in *Results*, we found the peak velocity of the slower component to be 0.176 ± 0.024 μm s^{-1} (n = 5), i.e., nearly identical to noise levels. We also found that QD adsorbed onto glass surface or in fixed cells showed speed distributions that were best fitted by a one-component function with a peak velocity of ~0.18 μm s^{-1} (data not shown), which was thought to be derived from instrumental noise. Thus, in differentiated 3T3L1 adipocytes, we fixed σ_1 at 0.182 μm s^{-1}, and the distributions were fitted using Eq. 4 by adjusting the values for A_1, A_2, and σ_2.

The MSD values were obtained with G-Track software, averaged over all trajectories in a cell, and then analyzed by fitting with the quadratic regression curve as

$$MSD(t) = (V_L t)^2 + 4Dt + C \quad (5)$$

where t, V_L, D, and C are time, apparent velocity of active transport, apparent diffusion coefficient, and instrumental noise, respectively (Saxton and Jacobson, 1997). As shown in Figure 4D, the active transport velocity within the TGN was thought to differ from those in other regions. Thus, the apparent velocity of active transport, V_L, is an averaged value of at least two different velocity components, and would be described as

$$V_L = \sqrt{pV_{stationary}^2 + (1-p)V_{rest}^2} \quad (6)$$

where p is the fraction of molecules exhibiting stationary behavior and $V_{stationary}$ and V_{rest} are velocities of stationary and other molecules, respectively. It seems reasonable to assume that the velocity of the stationary molecules ($V_{stationary}$) is ~0, because movement of most molecules within the *TGN* region was almost completely dependent on diffusion (see Figure 4D). Thus, we can calculate V_{rest} as

$$V_{rest} = V_L/\sqrt{1-p} \quad (7)$$

Myc-GLUT4 Translocation Assay and Western Blotting. GLUT4 translocation was analyzed as described previously (Nedachi and Kanzaki, 2006), with slight modification. In brief, 3T3L1 cells expressing myc-GLUT4-ECFP were serum starved and then incubated with or without the indicated concentrations of insulin. The cells were fixed with 1% paraformaldehyde/phosphate-buffered saline (PBS) and then subjected to cell-based enzyme-linked immunosorbent assay using anti-c-myc antibody, horseradish peroxidase-conjugated anti-mouse IgG antibody, and ortho-phenylendiamine for evaluating amounts of surface exposed myc-GLUT4-ECFP. Western blotting was performed as described previously (Nedachi and Kanzaki, 2006).

Statistical Analysis. Data are presented as means ± SD unless otherwise indicated. Statistical analyses were performed with the Mann–Whitney *U* test unless otherwise indicated, and p values of <0.05 are considered statistically significant.

RESULTS

Single Particle Tracking of GLUT4

To specifically demonstrate movement of a single GLUT4 by QD in 3T3L1 adipocytes, we used 3T3L1 clonal cell lines stably expressing GLUT4 with a myc-tag at the first exofacial loop and ECFP at the C terminus (myc-GLUT4-ECFP) (Nedachi and Kanzaki, 2006), and we labeled this protein very sparsely with 1.5 nM of a QD-conjugated Fab fragment of anti-myc antibody (Figure 1A; see *Materials and Methods* for details). This approach allowed us to track individual myc-GLUT4-ECFP movements as QD fluorescence (Supplemental Figure S1). We acquired fluorescent images for 10 s at 30 frames s^{-1} (Figure 1, B–D). We performed all experiments at precisely 30°C as maintaining constant temperature has been shown to be important for analyzing the kinetics of GLUT4 in living cell (Bai *et al*., 2007). Movements varied among individual GLUT4, with some staying in one position (Figure 1, C and D, traces 1 and 2), whereas others moved slowly (trace 3) or rapidly (trace 4). To quantitatively analyze movement, we calculated the GLUT4 velocity by linear fit of the movement during 4 frames. An example trajectory is shown in Figure 1E: the movement velocity was calculated (Figure 1F). The molecule was almost immobile initially (red) and then moved rapidly (green), stopped, and resumed moving again, although slowly (blue). A histogram showing these changes in velocity was constructed (Figure 1G).

It should be noted that, to evaluate potential disturbance of GLUT4 regulation caused by the QD labeling, we heavily labeled the myc-GLUT4-ECFP with 10-fold higher concentrations of the QD-conjugated Fab fragment of anti-myc antibody, and we confirmed that the QD-labeled myc-GLUT4-ECFP was colocalized with IRAP under basal state, which showed proper insulin-responsive translocation to plasma membrane assessed by a conventional confocal microscopy (Supplemental Figure S2). These results indicate that the QD-labeled myc-GLUT4-ECFP behaves similarly with endogenous GLUT4 and myc-GLUT4-ECFP as well as with IRAP in the absence or presence of insulin, implying the very sparsely labeled QD-myc-GLUT4-ECFP to be representative of entire intracellular GLUT4 pool, although we cannot rule out the possibility that QD labeling may influence their movements.

Static GLUT4 Sequestration and Insulin-responsive GLUT4 Dynamics

To analyze the impact of insulin on GLUT4 movements, we compared GLUT4 velocities before and after insulin stimulation (n = 5 cells). Under basal conditions, GLUT4 velocity displayed a skewed distribution, and insulin time-dependently shifted the distribution rightward (Figure 2A). Pretreatment with wortmannin, a phosphatidylinositol (PI) 3-kinase inhibitor well known to inhibit insulin-stimulated GLUT4 translocation, abolished the insulin action, and this wortmannin effect was reversible (Supplemental Figure S3A). Administering wortmannin to insulin-stimulated cells also partially but efficiently abrogated insulin-induced changes in GLUT4 movement (Supplemental Figure S3B). In addition to GLUT4, we also analyzed the movement of TfR, a well established marker for recycling pathway (Livingstone *et al*., 1996), with transferrin-QD conjugates in adipocytes. Interestingly, we found that movement of GLUT4 was significantly slower than that of TfR (Figure 2B). GLUT4 behavior in undifferentiated 3T3L1 fibroblasts differed strikingly from that in differentiated adipocytes, which showed very rapid movement with no significant velocity distribution change after insulin stimulation (Figure 2, C and D), although Akt phosphorylation was induced (Figure 2E). These results indicate that our method faithfully describes the relative velocities of GLUT4 in the basal and insulin-stimulated states of cells.

To quantitatively characterize in detail how insulin stimulation impacts GLUT4 behavior, we fitted the speed distributions with the prospective speed distribution function of two-dimensional movement (see Eq. 3 in *Materials and Methods*). The speed distributions, in fact, best fit the sum of two components (see Eq. 4 in *Materials and Methods*). In the basal state, the peak velocity of the slower component (σ_1) was 0.171 ± 0.017 μm s^{-1}, i.e., nearly identical to the noise levels of our instrumentation (6 nm/33 ms = 0.182 μm s^{-1}; see *Materials and Methods*; Watanabe and Higuchi, 2007). This observation shows the slower component to result from inevitable systemic noise fluctuation, such that the population seems to be essentially immobile. Thus, we defined two components, immobile and mobile, and fixed σ_1 of 0.182 μm s^{-1} as the immobile component velocity to further analyze the impact of insulin stimulation (Figure 3A).

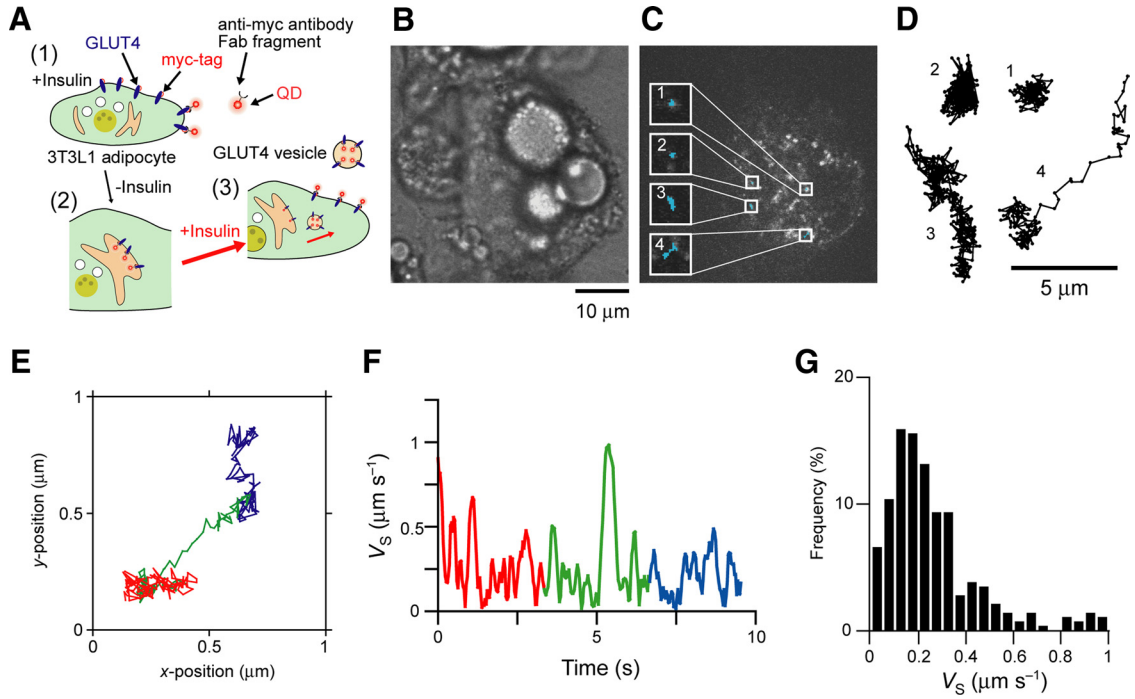

Figure 1. Movement of GLUT4 observed by QD fluorescence. (A) Procedure for labeling myc-GLUT4-ECFP with QD. First, cells were stimulated with insulin in the presence of a QD-conjugated Fab fragment of anti-myc antibody so that the myc-tag of the myc-GLUT4-ECFP molecule was exposed to the cell exterior and labeled with the antibody (1). Then, both insulin and anti-myc-QD were washed out, allowing the labeled GLUT4 molecule to be internalized and recycled back to the storage compartments (2). Thereafter, GLUT4 dynamics were observed by QD fluorescence with confocal or TIRF microscopes in the presence or absence of insulin (3). See *Materials and Methods* for details. (B and C) Bright field (B) and fluorescent (C) images of a differentiated 3T3L1 adipocyte labeled with anti-myc-QD. In C, some traces of GLUT4 molecule movement for 10 s (300 frames) are superimposed in blue. (D) Magnified traces depicted in C. (E) Example of movement of a GLUT4 molecule for 10 s. The trace is shown in different colors for each 100 frames (initial, middle, and last 100 frames shown in red, green, and blue, respectively). (F) Time course of the speed of the GLUT4 molecule shown in E. (G) Histogram of the speed of the GLUT4 molecule calculated in F. The average speed of this GLUT4 molecule for the 10-s period was 0.26 ± 0.20 μm s^{-1}.

The insulin-induced impact was not detected as a marked alteration in the peak velocity of the mobile phase (σ_2; basal: 0.378 ± 0.038 μm s^{-1}, insulin: 0.427 ± 0.050 μm s^{-1}; p = 0.14) in this analysis; however, significant changes in the fraction ratio of each phase were observed (Figure 3B). The immobile fraction accounted for 64 ± 14% in the basal state and then gradually dropped below 20% with 30-min insulin stimulation (18 ± 3%), producing a condition in which most GLUT4 was in the mobile fraction (Figure 3B). Wortmannin effects were also clearly illustrated by this procedure (Figure 3B). Akt substrate of 160 kDa (AS160) is known to be a wortmannin-sensitive downstream regulator of insulin signaling (Sano *et al*., 2003), and its T642 residue has been shown to function as a critical Akt-dependent phosphorylation site responsible for exerting insulin-induced GLUT4 translocation (Ramm *et al*., 2006). Therefore, we analyzed insulin actions in 3T3L1 adipocytes overexpressing T642A mutant version of AS160 and found that insulin failed to trigger acceleration of GLUT4 movement, resulting in no increase in mobile GLUT4 fraction in the cells (Figure 3B and Supplemental Figure S3C). Together, these data indicate that insulin increases GLUT4 number in the mobile phase in a PI 3-kinase/AS160-dependent manner.

Insulin Stimulation Releases the Immobilized GLUT4

To rule out the unlikely possibility that the insulin-dependent increase in the mobile GLUT4 is solely due to the increase in rapidly vibrating molecules within a confined region, we next used mean-square displacement (MSD) curves (Supplemental Figure 3C; Saxton and Jacobson, 1997). MSD curves of individual GLUT4 displayed diverse patterns in both basal and insulin-stimulated states, in which some showed random diffusion, whereas others showed directed transport or confined diffusion (data not shown). The averaged MSD values over all trajectories were analyzed with Eq. 5 (see *Materials and Methods*). Under basal conditions, MSD increased almost proportionally with a slight second-order component to the time elapsed (Figure 3C, black), suggesting GLUT4 movement in the basal state to be governed predominantly by diffusion. Insulin stimulation markedly increased both the contribution of active transport (*~3.5-fold*) and the apparent diffusion coefficient (*~2.5-fold*) (Figure 3C). Together, these data indicate that insulin stimulation increases the population of GLUT4 being released from the immobilized state.

Behavioral Characteristics of GLUT4 in the Perinuclear TGN and Other Regions in 3T3L1 Adipocytes

In 3T3L1 adipocytes, GLUT4 transport vesicles localized around the perinuclear TGN region are thought to be major GLUT4 storage compartment sites (Martinez-Arca *et al*., 2000; Shewan *et al*., 2003). We next separately analyzed GLUT4 movements in the perinuclear TGN region and other regions of the cell (Figure 4, A and B). Velocity analysis revealed a GLUT4 subset around the perinuclear TGN region remaining immobile even after 15 min of insulin stimulation (Figure 4C, blue; immobile:mobile = 61:39), whereas GLUT4 scattered in other regions constituted a clear mobile

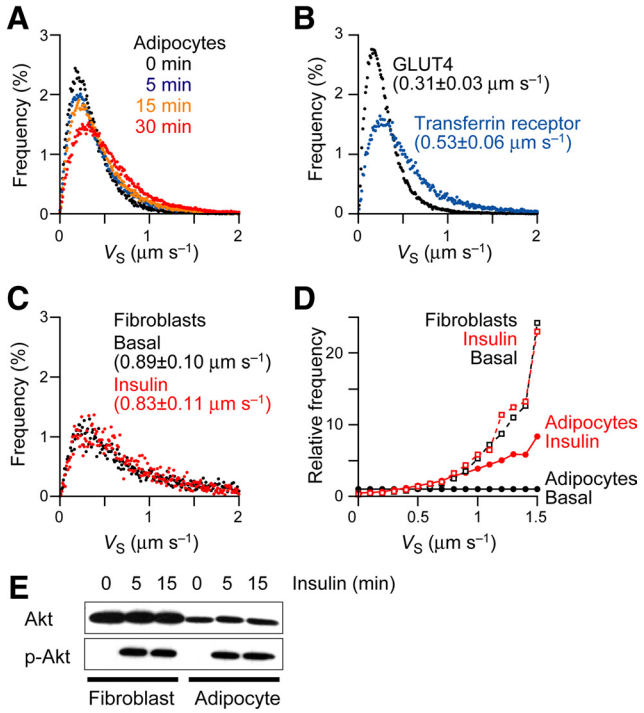

Figure 2. Tracking of GLUT4 in 3T3L1 cells. Insulin stimulation increases the population of fast moving GLUT4 only in 3T3L1 adipocytes (A) Velocity distributions of GLUT4 movement in differentiated 3T3L1 adipocytes before (black) and 5 min (blue), 15 min (orange), and 30 min (red) after stimulation with 100 nM insulin. The mean velocities were 0.34 ± 0.06, 0.45 ± 0.15*, 0.44 ± 0.11*, and 0.54 ± 0.08* μm s^{-1} before and 5, 15, and 30 min after insulin stimulation, respectively (n = 7). *$p < 0.05$ versus basal condition by Williams' multiple comparison. (B) Velocity distributions of GLUT4 (black) and transferrin receptor (blue) movement in differentiated adipocytes in the absence of insulin. The mean velocities are also shown (n = 11 for GLUT4, n = 7 for transferrin receptor; $p < 0.001$). (C) Velocity distributions of GLUT4 movement in undifferentiated 3T3L1 fibroblasts before (black) and 30 min (red) after stimulation with 100 nM insulin. The mean velocities are also shown (n = 6; p = 0.70). (D) For clear comparison between conditions A and C, relative velocity distributions of GLUT4 in differentiated 3T3L1 adipocytes (closed circles, solid line) and undifferentiated 3T3L1 fibroblasts (open squares, dashed line) before (black) and after (red) 30-min stimulation with 100 nM insulin are shown. (E) Western blot analysis of Akt and Ser^{473} phosphorylated Akt (p-Akt).

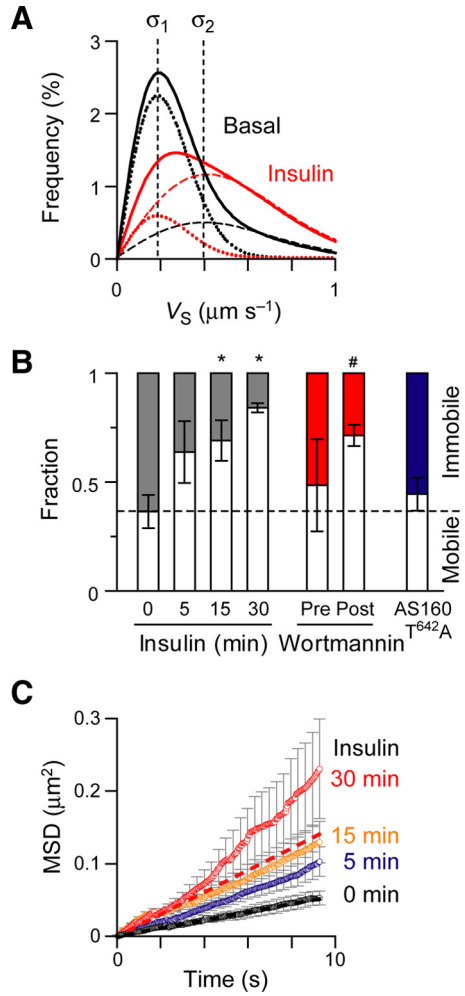

Figure 3. Quantitative analyses of GLUT4 movement in 3T3L1 adipocyte. (A) Speed distributions of GLUT4 molecules shown in Figure 2A were fitted by Eq. 4. Dotted lines, dashed lines and solid lines represent the immobile component, mobile component, and sum of the two components, respectively. Basal (black) and insulin-stimulated (30 min; red) data are shown. σ_1 and σ_2 are peak velocities of the immobile and mobile components, respectively. (B) Fractions of each moving component under the indicated conditions. White and colored columns represent immobile and mobile moving components, respectively. Data from Supplemental Figure S2 were used for pre- and posttreatment of wortmannin and T642A mutant of AS160. Data are means ± SEM, with *$p < 0.05$ and $^{\#}p < 0.05$ versus basal by Williams' and Dunnett's multiple comparison, respectively. (C) MSD curves before and after insulin stimulation (n = 5). Dashed lines represent the contribution of diffusion obtained from fitting with Eq. 5. Before insulin stimulation, $D = 1.5 \times 10^{-3}$ μm^{2}s^{-1} and $V_L = 0.9 \times 10^{-2}$ μm s^{-1}. After 30 min of insulin stimulation, $D = 3.8 \times 10^{-3}$ μm^{2}s^{-1} and $V_L = 3.2 \times 10^{-2}$ μm s^{-1}. Data are presented as means ± SEM.

fraction (Figure 4C, red; immobile:mobile = 27:73). The regional difference also was illustrated by MSD curves (Figure 4D). First, the GLUT4 diffusion coefficient around the *TGN* region was only 17% of that in other cell regions. Second, the active transport contribution was minimal in the TGN, whereas that in other regions was apparent (Figure 4D, dashed lines).

We next constructed a functional map of GLUT4 by using the diffusion coefficients of individual GLUT4. The GLUT4 movements after 15 min of insulin stimulation were classified into two groups using a diffusion coefficient cut-off value of 1.4×10^{-2} μm^2 s^{-1}, which is 2 times of SD (2SD) above the diffusion coefficient within the TGN region (SD = 0.5×10^{-2} μm^2 s^{-1}, n = 32; Figure 4, D and E, black line). The positions of GLUT4 were mapped on the cell image as mobile (red) and immobile (blue) groups (Figure 4F). In most cells, immobile GLUT4 (blue) assembled mainly around the perinuclear TGN region laterally surrounded by mobile GLUT4 (red), although there were a few immobile GLUT4 in peripheral regions.

Insulin Stimulation Increases Numbers of GLUT4-containing Vesicles Approaching the Plasma Membrane That Display Different Dwelling Characteristics

To examine whether insulin-responsive acceleration of intracellular GLUT4 dynamics contributes to making the plasma membrane more accessible, we next used our QD-based approach with total internal reflection fluorescence

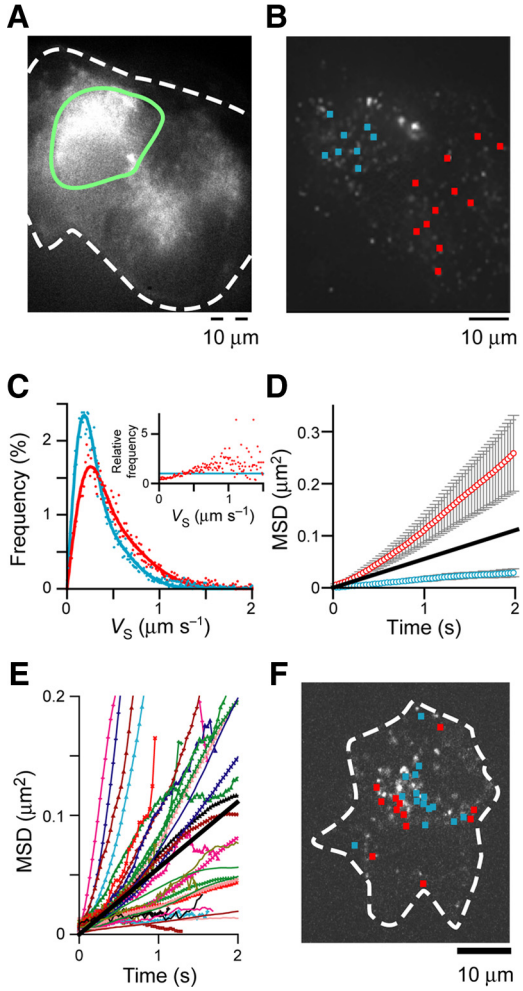

Figure 4. GLUT4 behaviors at the perinuclear TGN and other regions. (A and B) Fluorescent images of myc-GLUT4-ECFP (A) and QD605 (B). In A, the white dashed line represents the cell contour. Perinuclear TGN regions are shown surrounded by a green line. In B, traces of QD605-labeled myc-GLUT4-ECFP within the perinuclear-TGN (blue) and other (red) regions are superimposed. (C and D) Speed distributions (C) and MSD curves (D) of GLUT4 molecules shown in B. The apparent diffusion coefficients of GLUT4 within the perinuclear TGN and other regions were 0.4×10^{-2} μm^2 s^{-1} and 2.3×10^{-2} μm^2 s^{-1}, respectively. Black line represents MSD curve of a molecule with a diffusion coefficient of 1.4×10^{-2} μm^2 s^{-1} (2SD above diffusion coefficient within TGN; i.e., ~95% of molecules within TGN were expected to have diffusion coefficients below this value). In D, data are presented as means ± SEM. (E and F) Movements of GLUT4 molecules were classified into two groups by the MSD curves in E based on whether the diffusion coefficient was below or above 1.4×10^{-2} μm^2 s^{-1} (black) and then mapped on a cell image (F). GLUT4 molecules with high diffusion coefficients are mapped in red, whereas those with low diffusion coefficients are mapped in blue. White dashed line represents cell contour.

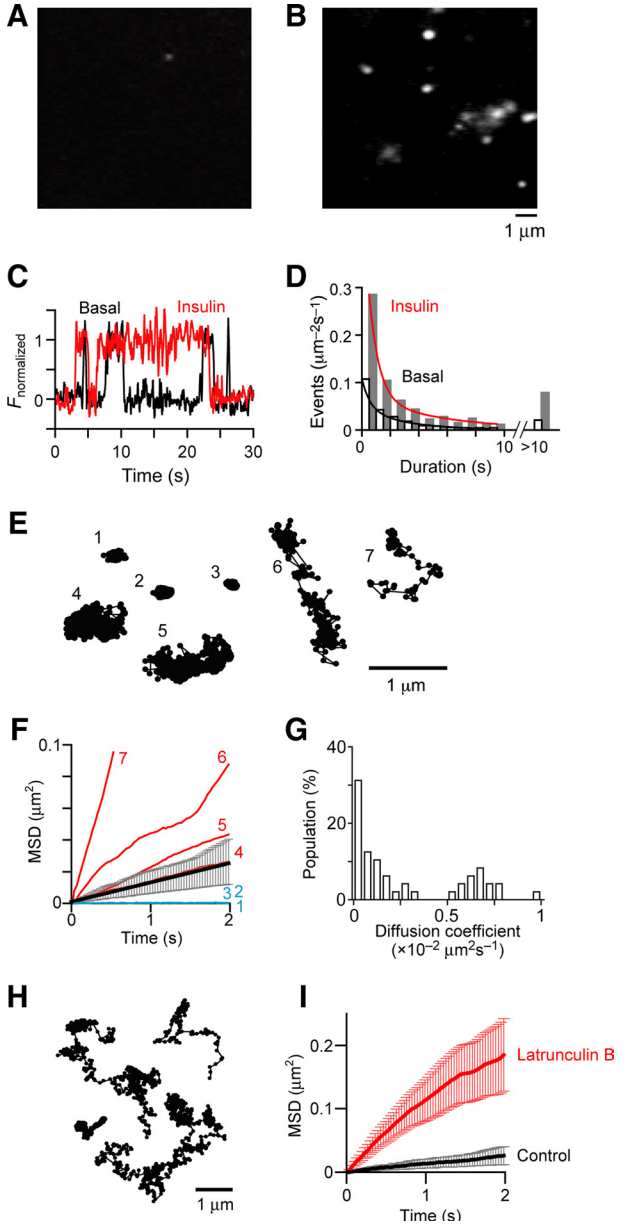

Figure 5. Analysis of GLUT4 dynamics beneath the plasma membrane by TIRF microscopy (A and B) TIRF images of QD fluorescence before (A) and after (B) insulin stimulation. (C) Example of time course of change in QD fluorescence. (D) Histogram of time spent by GLUT4 in the TIRF zone. Investigations of five cells showed event rates of QD signals approaching the TIRF zone to be (0.6 ± 0.3) $\times 10^{-2}$ and (2.2 ± 0.5) $\times 10^{-2}$ μm^{-2} s^{-1} before and after insulin stimulation ($p < 0.01$), and the mean durations in basal and insulin-stimulated states were 0.57 ± 0.07 and 0.83 ± 0.11 s, respectively ($p < 0.01$). Smooth lines are double-exponential curves. Time constants of the shorter component were 0.23 ± 0.07 and 0.34 ± 0.04 s ($p < 0.05$), and those of the longer component were 0.57 ± 0.07 and 0.83 ± 0.11 s ($p < 0.01$) in the absence and presence of insulin stimulation. (E and F) Typical traces and MSD curves of GLUT4 movement in the TIRF zone. The movement was roughly classified into two distinct groups, immobile (molecules 1–3; blue) and mobile (molecules 4–7; red). In F, black line represents averaged MSD curve. (G) Histogram of diffusion coefficient of GLUT4 movement in the TIRF zone. At least two distinct populations are apparently observed. (H) Examples of GLUT4 movement within the TIRF zone in 3T3L1 adipocytes treated with latrunculin B. (I) MSD curves of GLUT4 movement in the TIRF zone in 3T3L1 adipocytes treated with (red) or without (black) latruncurin B. Black line is the same as the averaged MSD curve shown in F. Note that the vertical scale is different from that in F.

(TIRF) microscopy (Figure 5, A–C). The event rate of QD signals approaching the TIRF zone (within ~200 nm from a glass surface) rose significantly, by ~3.7-fold, after 15 min of insulin stimulation (Figure 5D), and this insulin action was completely inhibited by wortmannin pretreatment (data not shown). The time GLUT4 remained within the TIRF zone was significantly prolonged by insulin stimulation, which could be fitted by double-exponential curves (Figure 5D). Importantly, the time constants seemed to both be signifi-

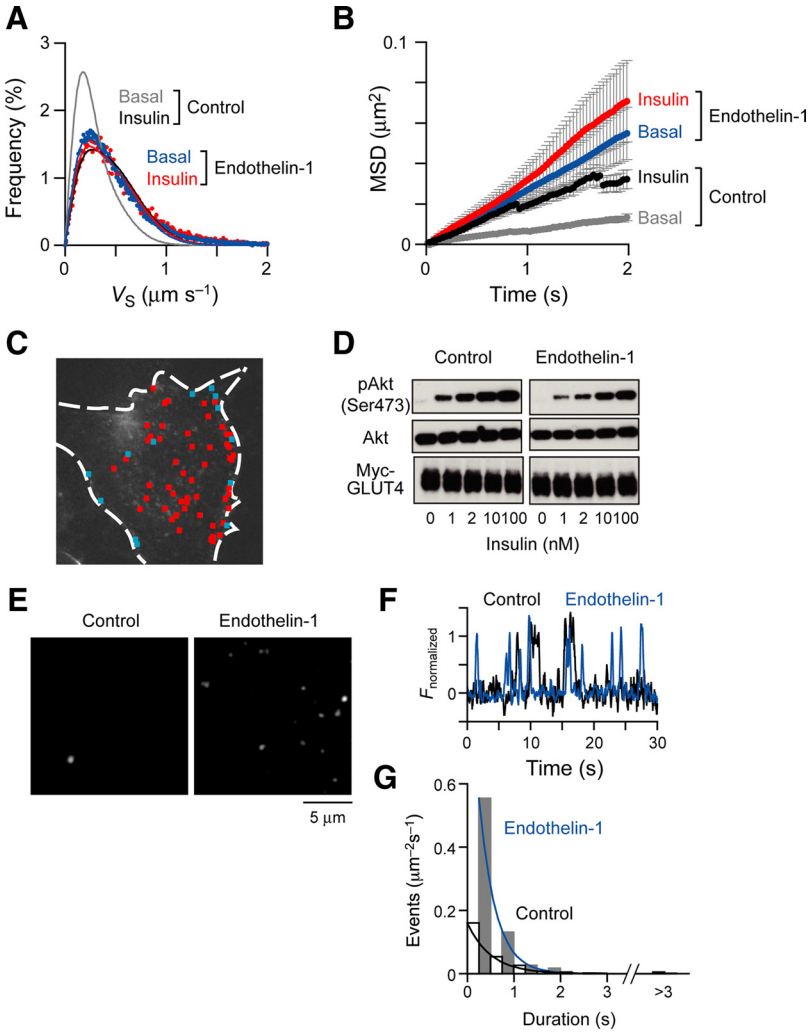

Figure 6. Effects of ET-1 on GLUT4 dynamics. (A and B) Speed distribution (A) and MSD curve (B) of GLUT4 movement in ET-1–treated 3T3L1 adipocytes without (blue) or with (red) insulin stimulation. Smooth lines are fitting curves based on Eq. 4. The apparent diffusion coefficient in the absence of insulin stimulation was 6.4×10^{-3} μm^2 s^{-1}. For comparison, values obtained from control cells are also shown. In B, data are presented as means ± SEM. (C) Maps of diffusion coefficients. Colors are the same as in Figure 4D. (D) Effects of ET-1 on insulin-induced phosphorylation of Akt (top) and expression levels of Akt (middle) and Myc-GLUT4-ECFP (bottom). (E) TIRF images of QD605-labeled GLUT4 in 3T3L1 adipocytes without (left) or with (right) ET-1 treatment. (F) Time course of the QD fluorescence change. (G) Histogram of time spent by GLUT4 in the TIRF zone. The event rates of QD signals approaching the TIRF zone were $(1.3 \pm 0.2) \times 10^{-2}$ and $(3.7 \pm 0.4) \times 10^{-2}$ μm^{-2} s^{-1} without versus with ET-1 treatment, respectively ($n = 4$; $p < 0.01$).

cantly increased by insulin stimulation. The trajectories of newly approaching GLUT4-containing vesicles under insulin-stimulated conditions could be roughly classified into two groups, staying in one position (Figure 5E, traces 1–3) and drifting in the TIRF zone (Figure 5E, traces 4–7). These observations are further represented by MSD curves showing a clear difference between the staying in one position (Figure 5F, blue) and the drifting (Figure 5F, red). A histogram constructed from the diffusion coefficient of each GLUT4 also revealed two peaks, indicating the presence of at least two distinct GLUT4 populations successfully captured in the TIRF zone (Figure 5G). The behavior of GLUT4-containing vesicles beneath the plasma membrane was dramatically altered in the presence of latrunculin B, an actin-disrupting reagent, as evidenced by the MSD curve (Figure 5, H and I), indicating cortical F-actin dynamics to be involved in regulation of tethering/docking processes of GLUT4-containing vesicles beneath the plasma membrane.

Behaviors of GLUT4 in Adipocytes in an Insulin-resistant State

Finally, we analyzed GLUT4 movements after chronic ET-1 treatment, which impairs insulin-stimulated GLUT4 translocation in 3T3L1 adipocytes (Ishibashi *et al.*, 2001; Strawbridge and Elmendorf, 2005; Usui *et al.*, 2005). Unexpectedly, mobile GLUT4 was markedly increased in ET-1–pretreated adipocytes even without insulin stimulation (Figure 6A, blue; immobile:mobile = 26:74), as confirmed by the MSD curve (Figure 6B, blue). Functional mapping of GLUT4 also clearly showed a subset of immobile GLUT4 to have largely disappeared (Figure 6C). Insulin failed to influence GLUT4 movements (Figure 6, A and B, red). Insulin-induced Akt phosphorylation was confirmed (Figure 6D, top), although there was a slight reduction in phosphorylation after ET-1 treatment, as reported previously (Ishibashi *et al.*, 2001). A significant increase in the event rate of QD signals approaching the TIRF zone was also observed regardless of insulin stimulation, whereas very few GLUT4 remained in the TIRF zone (Figure 6, E–G). It should be noted that we used cells exhibiting similar fluorescent profiles of intracellular QD signals for this comparison, to accurately evaluate the rate of approaching GLUT4 under each experimental condition.

DISCUSSION

Over the past several decades, considerable progress has been made in understanding the molecular basis of insulin receptor signals responsible for GLUT4 translocation (Watson *et al.*, 2004; Larance *et al.*, 2008). However, the actual steps responsive to insulin receptor signals and GLUT4 trafficking dynamics have yet to be clarified. This lack of progress is due at least in part to technical limitations of past

studies relying on GLUT4-fusing fluorescent proteins, e.g., enhanced green fluorescent protein (EGFP) (Kanzaki and Pessin, 2001), which is limited by dim fluorescence, and its sensitivity to photobleaching, which makes it unsuitable for investigating GLUT4 behavior at high spatial and temporal resolution. Although TIRF microscopic analysis of GLUT4-EGFP has been used to improve both spatial and temporal resolution, this system is limited to sites near the cell surface (Bai *et al.*, 2007; Huang *et al.*, 2007).

Our approach using QD to very sparsely label GLUT4 molecules reduces the highly complex regulation of GLUT4, by individually examining elements of GLUT4 movements in greater detail, thereby offering a novel solution to understanding functional steps of insulin-mediated GLUT4 trafficking. First, we provide direct evidence that in the absence of insulin stimulation "static retention" (Govers *et al.*, 2004) rather than "dynamic retention" (Karylowski *et al.*, 2004) is the major sequestration mechanism for GLUT4 that is endowed upon differentiation into mature adipocytes. Second, we quantitatively established that insulin stimulation alters GLUT4 behavior in at least three distinct steps. Third, we obtained compelling evidence that in the ET-1–induced insulin-resistant state, multiple steps of GLUT4 trafficking are altered.

Because visualization of the protein of interest in living cells requires modification of the native protein by tagging and/or labeling using a genetic engineering method (e.g., EGFP and myc-tag) and/or with specific antibodies conjugated with a fluorescent molecule (e.g., Qdot-labeled IgG), it is impossible to directly compare actual movements of native GLUT4 with QD–labeled myc-GLUT4-ECFP as tracked in the present study. However, our careful analysis of the overall behavioral characteristics of GLUT4 in the same cells before and after insulin stimulation support the insulin-responsive GLUT4 trafficking model depicted in Figure 7, as discussed below.

Behavioral Nature of GLUT4 in Storage Compartment(s) in Differentiated 3T3L1 Adipocytes

Based on our direct observation of intracellular GLUT4 and TfR behavior, we conclude that in the absence of insulin most GLUT4 are statically sequestered and their movements are spatially restricted to presumptive GLUT4 storage compartment(s) in fully differentiated 3T3L1 adipocytes. This stationary behavior of GLUT4 was not, however, observed in undifferentiated fibroblasts (Figure 2). Because GLUT4 ectopically expressed in undifferentiated 3T3L1 fibroblasts enter a general recycling pathway (El-Jack *et al.*, 1999) (Govers *et al.*, 2004), our single molecule tracking of GLUT4 faithfully pinpoints an important developmental alteration in the intracellular GLUT4 behavior that reflects interactions with a variety of GLUT4-/GLUT4-vesicle–associated molecules (Bogan *et al.*, 2003; Larance *et al.*, 2005). The stationary GLUT4 behavior occurring only in differentiated 3T3L1 adipocytes seems to be an important characteristic of GLUT4 storage compartment(s) that previous studies had characterized based mainly on morphological and biochemical properties (Livingstone *et al.*, 1996; Martin *et al.*, 1996, 2000).

Our data also indicate that in differentiated 3T3L1 adipocytes a small but significant fraction (~36%) of GLUT4 exists as a mobile phase in the basal state (Figure 3B). This small mobile fraction in the basal state may represent GLUT4 engaging in the general recycling pathway communicating with the cell surface that would account for GLUT4 being colocalized with the TfR (Livingstone *et al.*, 1996; Martin *et al.*, 1996). Nevertheless, this population did make a small contribution to the insulin stimulation of glucose uptake (Martin *et al.*, 1996). It is noteworthy that although the amount of GLUT4 with cell surface access is reportedly influenced by procedures for replating 3T3L1 adipocytes (Muretta *et al.*, 2008), possibly a deleterious factor leading to the two distinct retention models (Govers *et al.*, 2004; Karylowski *et al.*, 2004), our direct observations detected no significant changes in intracellular GLUT4 behavior even after replating procedures so long as the cells were fully differentiated (data not shown).

Insulin Signal Action Sites on the Process of GLUT4 Translocation in Differentiated 3T3L1 Adipocytes

Despite major advances in understanding the molecular basis of insulin receptor signals responsible for GLUT4 translocation (Kanzaki, 2006), the most fundamental unanswered

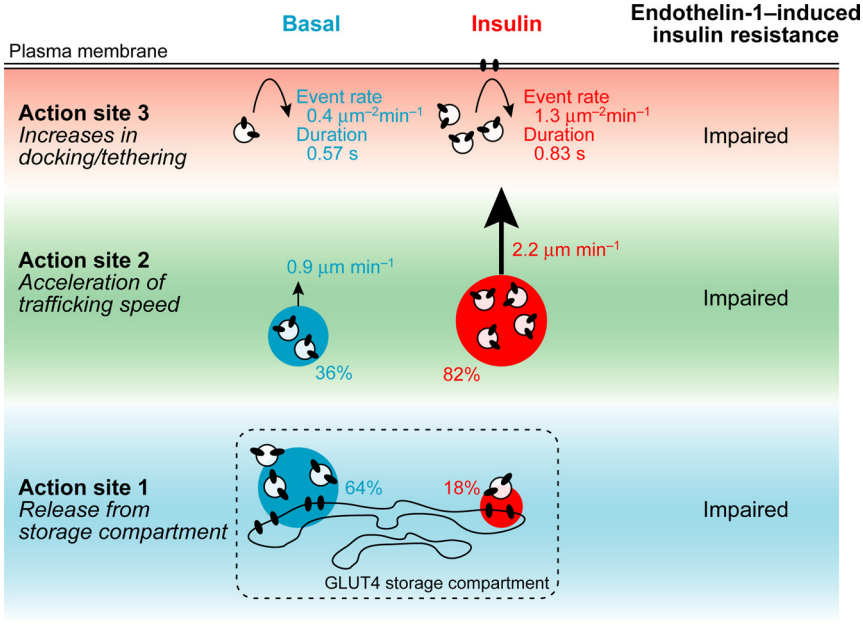

Figure 7. Quantification of GLUT4 trafficking and direct determination of insulin receptor signal action sites. Under basal conditions, the majority (64%) of GLUT4 exhibits stationary behavior (perhaps being sequestered with GLUT4 storage compartments), whereas the rest (36%) moves at an average speed 0.9 μm min^{-1}, contributing to a low frequency of events involving GLUT4-containing vesicles in the TIRF zone. After 30 min of insulin stimulation, only 18% of GLUT4 is stationary, whereas the majority (82%) now moves actively with an enhanced velocity of 2.2 μm min^{-1}, resulting in an ~3.7-fold increase in the frequency of GLUT4-containing vesicles with prolonged stays in the TIRF zone. Quantitative evaluation of GLUT4 behavior before and after insulin stimulation revealed at least three distinct steps to be significantly influenced by insulin stimulation, and behavioral properties of all three steps seemed to be aberrantly altered under insulin-resistant conditions elicited by chronic ET-1 treatment. Velocities were calculated by Eq. 7 shown in *Materials and Methods*.

question remains, i.e., what is the actual step(s) at which insulin signals directly converge and impact the process of dynamic GLUT4 trafficking events? By quantitatively comparing GLUT4 behavior before and after insulin stimulation, we directly defined at least three distinct points at which insulin stimulation alters GLUT4 behavior (Figure 7): 1) the release step from the putative GLUT4 anchoring system in storage compartment(s), 2) the speed at which transport vesicles containing GLUT4 move, and 3) the tethering/docking steps at the plasma membrane. Thus, our novel approach provides compelling answers that existing techniques lack the capacity to directly address, which are essential for further elucidating molecular basis of the insulin-responsive GLUT4 regulation.

A key observation in this set of experiments was that pretreatment with wortmannin, a PI 3-kinase inhibitor, abolished insulin-induced GLUT4 liberation, whereas once the cells were stimulated with insulin, posttreatment with wortmannin did not promptly restore the accelerated behavior to a quiescent state (Figure 3B and Supplemental Figure S3). A plausible explanation for these findings is that PI 3-kinase activity mediates the static sequestration of GLUT4 and/or other GLUT4-vesicle resident proteins such as IRAP from the poorly identified anchoring machinery in the storage compartments; however, once PI 3-kinase activity was extinguished, this anchoring system promptly resumed functioning, although it took some time until the released GLUT4 recycled back via an endocytic pathway en route to the GLUT4 storage compartments. This explanation is supported by our finding that overexpression of AS160/T642A, a dominant-interfering mutant version of AS160 (Ramm *et al*., 2006) functioning as a Rab-GTPase–activating protein regulated/phosphorylated by the PI 3-kinase–dependent Akt activation (Sano *et al*., 2003, 2007), abolished insulin-induced GLUT4 liberation (Figure 3B and Supplemental Figure S3C), although its underlying mechanisms involving AS160 remain to be further clarified. As discussed above, our detailed biophysical analyses suggest that in the absence of insulin GLUT4 molecules are physically sequestered in restricted cellular regions (so-called GLUT4 storage compartments) in fully differentiated 3T3L1 adipocytes. Sorting/targeting motifs on GLUT4 itself as well as those on resident proteins (Katagiri *et al*., 2002; Bogan *et al*., 2003; Ramm *et al*., 2006; Blot and McGraw, 2008; Song *et al*., 2008) might be involved in the establishment of stationary GLUT4 behavior that could be efficiently unleashed in response to the PI 3-kinase activity in a manner dependent upon AS160 phosphorylation, and this issue is the subject of ongoing studies.

We also demonstrated that insulin accelerated GLUT4 trafficking velocity, which supports previous reports showing that several motor proteins operate during GLUT4 translocation (Bose *et al*., 2002; Semiz *et al*., 2003; Yip *et al*., 2008). Because our current analysis does not distinguish among directions of GLUT4 movement, this point cannot be addressed unambiguously here and requires the development of new experimental approaches such as a three-dimensional imaging system (Watanabe *et al*., 2007). Although insulin stimulation of GLUT4 trafficking velocity apparently contributes to the acceleration of insulin-responsive GLUT4 translocation, insulin-responsive and wortmannin-sensitive GLUT4 liberation from the putative GLUT4 storage compartments could be more important as the primary impact of insulin signals because this event is prerequisite to enhanced GLUT4 delivery to the plasma membrane.

Evidence that once GLUT4 is released by insulin stimulation a relatively high level of GLUT4 trafficking activity persists even 15 min after wortmannin treatment (Figure 3B), a situation in which GLUT4 access to the plasma membrane is also still high, suggests that the plasma membrane is the site of another key regulatory step(s) attributable to the PI 3-kinase activity needed for exocytosis of GLUT4-containing vesicles. This notion is further supported by our observations with TIRF microscopy (Figure 5), consistent with other TIRF microscopy reports (Lizunov *et al*., 2005; Bai *et al*., 2007; Jiang *et al*., 2008). In this regard, AS160 has been implicated as a key regulator for exocytosis of GLUT4-containing vesicles (Bai *et al*., 2007; Jiang *et al*., 2008), although our finding described above provided a novel insight into role of AS160 in the regulation of intracellular GLUT4 behavior. In addition, because latrunculin treatment dramatically altered the behavior of GLUT4-containing vesicles beneath the plasma membrane (Figure 5F), cortical actin remodeling also apparently has a regulatory role in exocytosis of GLUT4-containing vesicles (Kanzaki and Pessin, 2001; Kanzaki, 2006; Lopez *et al*., 2009), although its mechanistic details as the insulin signal action site await further research.

Strikingly, our TIRF microscopic analysis using QD revealed that most arriving GLUT4-containing vesicles are instantly (~1 s) returned from the TIRF zone back to the intracellular space even after insulin stimulation (Figure 5), indicating that successful capture of arriving GLUT4-containing vesicles is a relatively rare event as has been observed with secretory vesicles in other cell types (Neher, 2006; Toonen *et al*., 2006). Although this phenomenon was partially observed in previous study using TIRF microscopy with GLUT4 fused to fluorescent protein (i.e., GLUT4-EGFP) as a probe (Bai *et al*., 2007), all the details have yet to be elucidated because high frequency of image acquisition is required for capturing such brief events, as we revealed in the present study. In addition, our novel approach using QD to very sparsely label GLUT4 allows us to accurately evaluate insulin-induced changes in event rate of newly approaching GLUT4-containing vesicles and their behaviors with very high spatial and temporal resolutions because there is little interference of excess background fluorescence emitted from the plasma membrane-integrated GLUT4-EGFP that is gradually increased after insulin stimulation. Using the above-mentioned novel capabilities, we revealed that insulin stimulation significantly increases numbers of GLUT4-containing vesicles approaching the plasma membrane that display different dwelling characteristics even at the very early time point of their visiting events (Figure 5). Although in the present study we did not focus on distinguishing between the docking/tethering and the final fusion events (thus physiological/functional significance of these behaviors of GLUT4 remain to be clarified), our data indicate the plasma membrane to be one of the functional sites of insulin signals in consistent with previous reports (Bai *et al*., 2007; Huang *et al*., 2007). In addition, our finding that the majority of GLUT4 is statically segregated inside cell keeping them away from the plasma membrane (TIRF zone) in the absence of insulin, implying the nature of arriving GLUT4-containing vesicles to be perhaps different between under basal and insulin-stimulated conditions (i.e., recycling endosomes containing both TfR and GLUT4 vs. the insulin-responsive GLUT4 storage vesicles). Thus, an intriguing possibility also emerges that arriving GLUT4-containing vesicles unleashed by insulin might endow with fundamentally distinct vesicle components that might be responsible for the different dwelling characteristics beneath the plasma membrane. In previous studies, insulin stimulation reduced the dwell duration of GLUT4-containing vesicles as a consequence of their facilitated exo-

cytosis (Bai *et al*., 2007; Huang *et al*., 2007), but these data obviously reflected the behavior of successfully captured, i.e., not "visiting," GLUT4-containing vesicles at the plasma membrane. Thus, our present data provide new insight into the earliest events at the plasma membrane. Details of the mechanisms underlying insulin-responsive regulation of this capturing step, which precedes tethering/docking processes, await further study.

Derangements in GLUT4 Behavior in the Insulin-resistant State Evoked by Chronic ET-1 Treatment in Differentiated 3T3L1 Adipocytes

We also have applied this approach to examining GLUT4 trafficking alterations in insulin-resistant states. Previous studies showed ET1-dependent insulin resistance to result from defects in insulin receptor signal transduction as well as from impaired cortical F-actin remodeling (Ishibashi *et al*., 2001; Strawbridge and Elmendorf, 2005; Usui *et al*., 2005). However, our data revealed that behavioral properties of GLUT4 both intracellularly and beneath the plasma membrane are also severely deranged in the insulin-resistant state (Figure 6). Surprisingly, there was unexpectedly high trafficking activity of GLUT4, associated with the disappearance of stationary GLUT4 storage compartments, even in the absence of insulin in ET-1–pretreated 3T3L1 adipocytes (Figure 6, A–C). Because ET-1 has been shown to acutely, although weakly, induce GLUT4 translocation in 3T3L1 adipocytes (Wu-Wong *et al*., 1999; Park *et al*., 2001), the higher GLUT4 mobility might be a consequence of chronic ET-1 treatment whereby GLUT4 are continuously released from the stationary GLUT4 storage compartment. Alternatively, in the presence of ET-1 the liberated GLUT4 might not gain access to stationary GLUT4 storage compartments, possibly due to malfunction of its anchoring machinery. In any case, despite the subsequent higher accessibility of GLUT4-containing vesicles to the TIRF zone (Figure 6, E–G), successful exocytosis was not achieved (data not shown) (Ishibashi *et al*., 2001; Strawbridge and Elmendorf, 2005; Usui *et al*., 2005) and this coincided with aberrant alterations (reduction) in dwell time profiles due to shorter stays within the TIRF zone (Figure 6, E–G), suggesting the machinery, including cortical actin remodeling, required for efficiently capturing GLUT4-containing vesicles to also be deranged. Thus, our data raise the possibility that, in certain insulin-resistant states, derangements in GLUT4 behavior can impair insulin-responsive GLUT4 translocation. This mechanism would operate in addition to the established insulin receptor signaling defects associated with insulin resistance, providing us with new insight into the pathophysiology of type 2 diabetes.

ACKNOWLEDGMENTS

We thank Dr. Taku Nedachi for generating the 3T3L1 clones and Fumie Wagatsuma and Natsumi Emoto for technical assistance. We also thank Prof. Jeffrey E. Pessin (Albert Einstein College of Medicine, Bronx, NY) for critical reading of the manuscript and valuable suggestions. This study was supported by Special Coordination Funds for Promoting Science and Technology, and also in part by grants from the Ministry of Education, Science, Sports and Culture of Japan and the New Energy and Industrial Technology Development Organization. H. Hatakeyama is a Research Fellow of the Japan Society for the Promotion of Science.

REFERENCES

Ariga, M., Nedachi, T., Katagiri, H., and Kanzaki, M. (2008). Functional role of sortilin in myogenesis and development of insulin-responsive glucose transport system in C2C12 myocytes. J. Biol. Chem. *283*, 10208–10220.

Bai, L., Wang, Y., Fan, J., Chen, Y., Ji, W., Qu, A., Xu, P., James, D. E., and Xu, T. (2007). Dissecting multiple steps of GLUT4 trafficking and identifying the sites of insulin action. Cell Metab. *5*, 47–57.

Birnbaum, M. J. (1989). Identification of a novel gene encoding an insulin-responsive glucose transporter protein. Cell *57*, 305–315.

Blot, V., and McGraw, T. E. (2008). Molecular mechanisms controlling GLUT4 intracellular retention. Mol. Biol. Cell *19*, 3477–3487.

Bogan, J. S., Hendon, N., McKee, A. E., Tsao, T. S., and Lodish, H. F. (2003). Functional cloning of TUG as a regulator of GLUT4 glucose transporter trafficking. Nature *425*, 727–733.

Bose, A., Guilherme, A., Robida, S. I., Nicoloro, S. M., Zhou, Q. L., Jiang, Z. Y., Pomerleau, D. P., and Czech, M. P. (2002). Glucose transporter recycling in response to insulin is facilitated by myosin Myo1c. Nature *420*, 821–824.

Cushman, S. W., and Wardzala, L. J. (1980). Potential mechanism of insulin action on glucose transport in the isolated rat adipose cell. J. Biol. Chem. *255*, 4758–4762.

Dahan, M., Levi, S., Luccardini, C., Rostaing, P., Riveau, B., and Triller, A. (2003). Diffusion dynamics of glycine receptors revealed by single-quantum dot tracking. Science *302*, 442–445.

El-Jack, A. K., Kandror, K. V., and Pilch, P. F. (1999). The formation of an insulin-responsive vesicular cargo compartment is an early event in 3T3-L1 adipocyte differentiation. Mol. Biol. Cell *10*, 1581–1594.

Govers, R., Coster, A. C., and James, D. E. (2004). Insulin increases cell surface GLUT4 levels by dose dependently discharging GLUT4 into a cell surface recycling pathway. Mol. Cell Biol. *24*, 6456–6466.

Huang, S., Lifshitz, L. M., Jones, C., Bellve, K. D., Standley, C., Fonseca, S., Corvera, S., Fogarty, K. E., and Czech, M. P. (2007). Insulin stimulates membrane fusion and GLUT4 accumulation in clathrin coats on adipocyte plasma membranes. Mol. Cell Biol. *27*, 3456–3469.

Ishibashi, K. I., Imamura, T., Sharma, P. M., Huang, J., Ugi, S., and Olefsky, J. M. (2001). Chronic endothelin-1 treatment leads to heterologous desensitization of insulin signaling in 3T3–L1 adipocytes. J. Clin. Invest. *107*, 1193–1202.

James, D. E., Brown, R., Navarro, J., and Pilch, P. F. (1988). Insulin-regulatable tissues express a unique insulin-sensitive glucose transport protein. Nature *333*, 183–185.

Jiang, L., Fan, J., Bai, L., Wang, Y., Chen, Y., Yang, L., Chen, L., and Xu, T. (2008). Direct quantification of fusion rate reveals a distal role for AS160 in insulin-stimulated fusion of GLUT4 storage vesicles. J. Biol. Chem. *283*, 8508–8516.

Kanzaki, M. (2006). Insulin receptor signals regulating GLUT4 translocation and actin dynamics. Endocr. J. *53*, 267–293.

Kanzaki, M., and Pessin, J. E. (2001). Insulin-stimulated GLUT4 translocation in adipocytes is dependent upon cortical actin remodeling. J. Biol. Chem. *276*, 42436–42444.

Karylowski, O., Zeigerer, A., Cohen, A., and McGraw, T. E. (2004). GLUT4 is retained by an intracellular cycle of vesicle formation and fusion with endosomes. Mol. Biol. Cell *15*, 870–882.

Katagiri, H., Asano, T., Yamada, T., Aoyama, T., Fukushima, Y., Kikuchi, M., Kodama, T., and Oka, Y. (2002). Acyl-coenzyme A dehydrogenases are localized on GLUT4-containing vesicles via association with insulin-regulated aminopeptidase in a manner dependent on its dileucine motif. Mol. Endocrinol. *16*, 1049–1059.

Larance, M., Ramm, G., and James, D. E. (2008). The GLUT4 code. Mol. Endocrinol. *22*, 226–233.

Larance, M., *et al*. (2005). Characterization of the role of the Rab GTPase-activating protein AS160 in insulin-regulated GLUT4 trafficking. J. Biol. Chem. *280*, 37803–37813.

Livingstone, C., James, D. E., Rice, J. E., and Gould, G. W. (1996). Compartment ablation analysis of the insulin-responsive glucose transporter (GLUT4) in 3T3L1 adipocytes. Biochem. J. *315*, 487–495.

Lizunov, V. A., Matsumoto, H., Zimmerberg, J., Cushman, S. W., and Frolov, V. A. (2005). Insulin stimulates the halting, tethering, and fusion of mobile GLUT4 vesicles in rat adipose cells. J. Cell Biol. *169*, 481–489.

Lopez, J. A., Burchfield, J. G., Blair, D. H., Mele, K., Ng, Y., Vallotton, P., James, D. E., and Hughes, W. E. (2009). Identification of a distal GLUT4 trafficking event controlled by actin polymerization. Mol. Biol. Cell *20*, 3918–3929.

Martin, S., Millar, C. A., Lyttle, C. T., Meerloo, T., Marsh, B. J., Gould, G. W., and James, D. E. (2000). Effects of insulin on intracellular GLUT4 vesicles in adipocytes: evidence for a secretory mode of regulation. J. Cell Sci. *113*, 3427–3438.

Martin, S., Tellam, J., Livingstone, C., Slot, J. W., Gould, G. W., and James, D. E. (1996). The glucose transporter (GLUT-4) and vesicle-associated membrane protein-2 (VAMP-2) are segregated from recycling endosomes in insulin-sensitive cells. J. Cell Biol. *134*, 625–635.

Martinez-Arca, S., Lalioti, V. S., and Sandoval, I. V. (2000). Intracellular targeting and retention of the glucose transporter GLUT4 by the perinuclear storage compartment involves distinct carboxyl-tail motifs. J. Cell Sci. *113*, 1705–1715.

Muretta, J. M., Romenskaia, I., and Mastick, C. C. (2008). Insulin releases Glut4 from static storage compartments into cycling endosomes and increases the rate constant for Glut4 exocytosis. J. Biol. Chem. *283*, 311–323.

Nedachi, T., and Kanzaki, M. (2006). Regulation of glucose transporters by insulin and extracellular glucose in C2C12 myotubes. Am. J. Physiol. Endocrinol. Metab. *291*, E817–E828.

Neher, E. (2006). A comparison between exocytic control mechanisms in adrenal chromaffin cells and a glutamatergic synapse. Pflugers Arch. *453*, 261–268.

Park, J. G., Bose, A., Leszyk, J., and Czech, M. P. (2001). PYK2 as a mediator of endothelin-1/G alpha 11 signaling to GLUT4 glucose transporters. J. Biol. Chem. *276*, 47751–47754.

Ramm, G., Larance, M., Guilhaus, M., and James, D. E. (2006). A role for 14–3-3 in insulin-stimulated GLUT4 translocation through its interaction with the RabGAP AS160. J. Biol. Chem. *281*, 29174–29180.

Sano, H., Eguez, L., Teruel, M. N., Fukuda, M., Chuang, T. D., Chavez, J. A., Lienhard, G. E., and McGraw, T. E. (2007). Rab10, a target of the AS160 Rab GAP, is required for insulin-stimulated translocation of GLUT4 to the adipocyte plasma membrane. Cell Metab. *5*, 293–303.

Sano, H., Kane, S., Sano, E., Miinea, C. P., Asara, J. M., Lane, W. S., Garner, C. W., and Lienhard, G. E. (2003). Insulin-stimulated phosphorylation of a Rab GTPase-activating protein regulates GLUT4 translocation. J. Biol. Chem. *278*, 14599–14602.

Saxton, M. J., and Jacobson, K. (1997). Single-particle tracking: applications to membrane dynamics. Annu. Rev. Biophys. Biomol. Struct. *26*, 373–399.

Semiz, S., Park, J. G., Nicoloro, S. M., Furcinitti, P., Zhang, C., Chawla, A., Leszyk, J., and Czech, M. P. (2003). Conventional kinesin KIF5B mediates insulin-stimulated GLUT4 movements on microtubules. EMBO J. *22*, 2387–2399.

Serge, A., Bertaux, N., Rigneault, H., and Marguet, D. (2008). Dynamic multiple-target tracing to probe spatiotemporal cartography of cell membranes. Nat. Methods *5*, 687–694.

Shepherd, P., and Khan, B. (1999). Glucose transporters and insulin action. N. Engl. J. Med. *341*, 248–257.

Shewan, A. M., van Dam, E. M., Martin, S., Luen, T. B., Hong, W., Bryant, N. J., and James, D. E. (2003). GLUT4 recycles via a trans-Golgi network (TGN) subdomain enriched in Syntaxins 6 and 16 but not TGN *38*, involvement of an acidic targeting motif. Mol. Biol. Cell *14*, 973–986.

Shigematsu, S., Khan, A. H., Kanzaki, M., and Pessin, J. E. (2002). intracellular insulin-responsive glucose transporter (GLUT4) distribution but not insulin-stimulated GLUT4 exocytosis and recycling are microtubule dependent. Mol. Endocrinol. *16*, 1060–1068.

Shigematsu, S., Watson, R. T., Khan, A. H., and Pessin, J. E. (2003). The adipocyte plasma membrane caveolin functional/structural organization is necessary for the efficient endocytosis of GLUT4. J. Biol. Chem. *278*, 10683–10690.

Song, X. M., Hresko, R. C., and Mueckler, M. (2008). Identification of amino acid residues within the C terminus of the Glut4 glucose transporter that are essential for insulin-stimulated redistribution to the plasma membrane. J. Biol. Chem. *283*, 12571–12585.

Strawbridge, A. B., and Elmendorf, J. S. (2005). Phosphatidylinositol 4,5-bisphosphate reverses endothelin-1-induced insulin resistance via an actin-dependent mechanism. Diabetes *54*, 1698–1705.

Suzuki, K., and Kono, T. (1980). Evidence that insulin causes translocation of glucose transport activity to the plasma membrane from an intracellular storage site. Proc. Natl. Acad. Sci. USA *77*, 2542–2545.

Tada, H., Higuchi, H., Wanatabe, T. M., and Ohuchi, N. (2007). In vivo real-time tracking of single quantum dots conjugated with monoclonal anti-HER2 antibody in tumors of mice. Cancer Res. *67*, 1138–1144.

Toonen, R. F., Kochubey, O., de Wit, H., Gulyas-Kovacs, A., Konijnenburg, B., Sorensen, J. B., Klingauf, J., and Verhage, M. (2006). Dissecting docking and tethering of secretory vesicles at the target membrane. EMBO J. *25*, 3725–3737.

Usui, I., Imamura, T., Babendure, J. L., Satoh, H., Lu, J. C., Hupfeld, C. J., and Olefsky, J. M. (2005). G protein-coupled receptor kinase 2 mediates endothelin-1-induced insulin resistance via the inhibition of both Galphaq/11 and insulin receptor substrate-1 pathways in 3T3–L1 adipocytes. Mol. Endocrinol. *19*, 2760–2768.

Watanabe, T. M., and Higuchi, H. (2007). Stepwise movements in vesicle transport of HER2 by motor proteins in living cells. Biophys. J. *92*, 4109–4120.

Watanabe, T. M., Sato, T., Gonda, K., and Higuchi, H. (2007). Three-dimensional nanometry of vesicle transport in living cells using dual-focus imaging optics. Biochem. Biophys. Res. Commun. *359*, 1–7.

Watson, R. T., Kanzaki, M., and Pessin, J. E. (2004). Regulated membrane trafficking of the insulin-responsive glucose transporter 4 in adipocytes. Endocr. Rev. *25*, 177–204.

Wu-Wong, J. R., Berg, C. E., Wang, J., Chiou, W. J., and Fissel, B. (1999). Endothelin stimulates glucose uptake and GLUT4 translocation via activation of endothelin ETA receptor in 3T3–L1 adipocytes. J. Biol. Chem. *274*, 8103–8110.

Yip, M. F., Ramm, G., Larance, M., Hoehn, K. L., Wagner, M. C., Guilhaus, M., and James, D. E. (2008). CaMKII-mediated phosphorylation of the myosin motor Myo1c is required for insulin-stimulated GLUT4 translocation in adipocytes. Cell Metab. *8*, 384–398.